FY-2005 Summary Report:

Ion Irradiation Study on Microstructure Stability of GFR Ceramics:
ZrC, ZrN, TiC, TiN and SiC
Irradiated with 1 MeV Kr Ions to 10 and 70 dpa at 800ºC

Jian. Gan[1], Randall S. Fielding[1], Mitchell K. Meyer[1] and Robert C. Birtcher[2]

[1]Idaho National Laboratory, Idaho Falls, ID
[2]Argonne National Laboratory

September 27, 2005

Abstract:

This is a 1-year program to investigate the microstructural changes in ZrN, TiC, TiN and SiC due to heavy ion irradiation under conditions relevant to gas-cooled fast reactors (GFR). The previous work on ZrC (FY-2004) is included for comparison and discussion. TEM disc samples of hot-pressed ZrC, ZrN, TiC, TiN (all in NaCl type structure) and SiC (6H-SiC type) were irradiated using 1 MeV Kr ions at 800°C. The irradiations were conducted at a dose rate of approximately 3.0×10^{-3} dpa/s with doses up to 70 dpa. Post-irradiation examination reveals the changes in microstructure due to Kr ion irradiation. Lattice increase is observed for the irradiated samples at 70 dpa. No evidence of faulted loops or amorphization is found in these ceramics. Voids are found in TiC with an estimated swelling of approximately 0.01%. Dislocation networks and perfect loops are found in TiC and TiN. SiC shows well-developed loops at 70 dpa. An ordered microstructure was found in ZrN. The results show that SiC, TiC and TiN perform better than ZrC and ZrN on microstructural response to Kr ion irradiation at 800ºC.

Introduction:

Refractory ceramics have been considered for the gas cooled fast reactor (GFR). The fuel for the GFR requires both a high heavy metal loading and the ability to withstand temperatures of approximately 1200°C under normal operation and up to 1600ºC during a loss of coolant accident. Current gas reactor fuel technology is not adaptable to a gas-cooled fast reactor. The categories of fuel with the highest potential for success are carbide and nitride-based composite-type fuels. These fuels consist of a fissile phase dispersed within a refractory matrix. Potential fuel matrix materials are limited to those with low neutron absorption (thus excluding refractory metals), high melting temperatures (> 2000°C), and tolerance to high dose irradiation damage from neutrons and fission products. Refractory ceramics of ZrC, ZrN, TiC, TiN and SiC are candidates for matrix materials for dispersion type fuel due to their neutronic performance, thermal properties, chemical behavior, crystal structure, and physical properties. The transition metal carbides and nitrides (ZrC, ZrN, TiC and TiN) have a NaCl type FCC structure. The 6H-

SiC is a common form of SiC that has a hexagonal structure. The high dose, high-temperature radiation effects on the microstructure of these ceramics have not been explored previously.

A comprehensive review of radiation effects in ceramics can be found in the reference [1]. A limited number of ZrC TRISO-type fuel particles have been irradiated with neutrons at 900°C to a low burnup (~1.6 dpa) [2]. Optical examination of the cross section of the irradiated fuel particles did not reveal any mechanical failure of ZrC coating (~70 µm thick) although no detailed postirradiation microstructural analysis of the ZrC was performed. Data for ZrC has been generated under a limited range of irradiation conditions [3,4]. These studies showed a ZrC lattice parameter increase at neutron fluences of ~$1.5x10^{20}$ n/cm^2 (~0.2 dpa) at 50, 150 and 1100°C with lattice increases of 0.26%, 0.46% and 0.13%, respectively. The work by Keilholtz et al [5] on ZrC irradiated with neutrons at 300-700°C suggests the mechanism of lattice expansion is defect agglomeration. They reported a measured volume increase of approximately 3% at doses of ~ 3 dpa and remained saturated up to a dose of 8 dpa. Their calculated volume increase from ~0.5% lattice expansion was about 50% of the measured volume increase at doses of 3~8 dpa. There is no microstructural characterization for neutron irradiated ZrC reported in the open literature.

The work by Dyslin, et al. on ZrC and TiC irradiated in the Engineering Test Reactor (ETR) at temperature of 130-355ºC to a dose of ~7.5 dpa showed a volume increase of 2.5% and 2.0% for ZrC and TiC, respectively [6]. Their thermal annealing studies of the irradiated ceramics indicated a greater shrinkage effect on TiC than on ZrC, suggesting a larger fraction of single defects in TiC. The smaller volume change in TiC was attributed to the smaller fraction of defect clusters compared to ZrC. The single defects are believed to cause less volume increase than clusters and are relatively easier to be annealed out.

SiC is one of the special materials that has attracted a lot interest due to its electronic properties, thermal stability, extreme hardness and chemical inertness. The work by Weber, et al., [7] on single crystal 6H-SiC irradiated in-situ along [0001] orientation with 1.5 MeV Xe ions at low temperatures (20k~475k) revealed that the material becomes completely amorphous at a dose of 0.25 dpa at T=20k. They found the critical temperature above which amorphization does not occur is 485k. Persson et al., reported their work on 4H-SiC implanted with 180 KeV Al ions at 600°C to doses of 1.3~$7.8x10^{14}$ cm^{-2}. They found loops at doses above $2.6x10^{14}$ ions/cm^2 and the loops reside on (0001) basal plan with average size of approximately 50 nm [8]. They also reported that the loops in 4H-SiC consist of C or Si self-interstitials, or both [9].

This work investigated the microstructural response of ZrC, ZrN, TiC, TiN and SiC irradiated with 1.0 MeV Kr ions to doses of 10 and 70 dpa at 800ºC with a damage rate of approximately $3.0x10^{-3}$ dpa/s. Considering the need to increase the temperature for the high dose rate to produce effective damage, the temperature used for heavy ion irradiation may not be representative of the same temperature in neutron irradiation. The large ratio of surface to volume has always been a concern for irradiation of thin foil using TEM disc samples. Nevertheless, heavy ion irradiation in an electron microscope using TEM samples offers the opportunity to perform low-cost irradiation studies on a wide range of materials that simulate some important aspects of the fission neutron environment. The result for a specific material from heavy ion irradiation of a TEM sample is not expected to be the same as for neutron

irradiation. However, a comparison of the microstructural response for materials under the same irradiation condition using this technique should provide valuable information on the relative performance of the materials.

Experiments

Commercially produced ZrC, ZrN, TiC, TiN and α-SiC samples, by vacuum hot pressing of powders then machining to form rods, were used in this work. The ceramics were received as 20 mm long rods with a diameter of 3 mm. Their chemical composition is listed in Table 1. The densities of ceramic rods were measured using both dimension and immersion methods. Porosity in the microstructure was examined using scanning electron microscopy (SEM). The 3 mm diameter discs with a thickness of 200 μm were cut using a low speed diamond saw. These disc samples were then wet-polished down to a thickness of ~100 μm. The discs were then mechanically dimpled from both sides to a thickness approximately 10~20 μm in the middle, followed by precision ion milling with 5.0 KeV argon ions at an incident angle of 5~7 degree.

Table 1. Chemical composition of the refractory ceramics (wt%)

	Zr	Ti	Si	Hf	Zn	W	C	N	O	Others	Ratio*
ZrC	**84.8**	0.19	<0.001	1.91	<0.02	<0.1	**11.3**	0.61	0.21	<0.1	1.01
ZrN	**87.6**	0.095	0.007	<0.02	<0.02	0.19	0.76	**11.4**	1.43	<0.1	0.85
TiC	<0.02	**80.2**	0.007	<0.02	0.17	<0.05	**19.4**	0.057	0.51	<0.02	0.97
TiN	<0.02	**78.9**	0.001	<0.02	<0.02	<0.05	0.58	**22.0**	0.46	<0.02	0.95
SiC	<0.005	<0.1	**62.08**	<0.005	<0.001	<0.05	**29.6**	0.35	0.58	Al_1.44 Fe_0.65	1.11

* The atomic ratio of the major element C or N to Zr, Ti or Si.

The irradiation was conducted with 1.0 MeV Kr ions using an intermediate voltage electron microscope (IVEM) equipped with a Tandem accelerator at Argonne National Laboratory. TEM disc samples were irradiated at 800ºC to 10 and 70 dpa except for TiN that was only irradiated to 70 dpa. Beam diameter for Kr ions was approximately 2 mm. Irradiation dose was calculated using TRIM program [10]. Dose rate is approximately 3.0×10^{-3} dpa/s with a pressure of less than than 7×10^{-8} torr. During the irradiation, the electron microscope was operated at 300 kV. The microstructural evolution was monitored on a TV screen and recorded on videotape.

Post-irradiation microstructure characterization was conducted at INL using a JEOL2010 transmission electron microscope operated at 200 kV. The features of irradiated microstructure such as loops, dislocation network, cavities and precipitates were examined. Diffraction patterns at zone [011] or [001] were used to determine the changes in lattice constant for material with FCC structure. Two beam diffraction at g=(200) is used for bright field imaging of dislocations and loops while rel-rod dark filed imaging is used to examine if faulted loops were present. For the hexagonal 6H-SiC, the diffraction patters at zone [1,-2,1,0] and [0,2,-2,-1] are used to determine the possible lattice expansion while the diffraction of (0,0,6) or (2,-1,6) near zone [0,-1,1,0] are used for the loops. The high resolution images for 6H-SiC basal plane projection are obtained at zone [1,-2,1,0] either without objective aperture or using the largest objective aperture.

Results:

Results of density measurement are listed in Table 2 along with the theoretical density of these ceramics for comparison [11,12]. The Hf (~2 wt.%) in ZrC and the porosity in TiN, Figure 1, is responsible for the unexpected high relative-density for ZrC and low relative-density for TiN, respectively. General features of the unirradiated microstructure for all 4 refractory ceramics are the uniformly distributed small defect clusters caused by ion milling damage during sample preparation. Bubbles at a size of approximately ~ 1 nm were found in the unirradiated samples. Although the number density of bubbles decreased and a slight size increase was observed, voids were not found in the irradiated ZrC, ZrN and TiN. A general observation for radiation-induced microstructural changes was an increase in the lattice constant and the lack of faulted loops at 70 dpa. The following sections provide the microstructure analysis for these ceramics before and after irradiation with Kr ions at 800ºC.

Table 2. Results of density measurement for as-received ceramics (g/cm^3)

Ceramics	By dimension	By immersion	Theoretic	Imm./Theoretic (%)
ZrC	6.59	6.58	6.48	101.5
ZrN	7.06	7.06	7.30	96.7
TiC	4.84	4.84	4.90	98.8
TiN	4.43	4.92	5.39	91.3
SiC	3.18	3.19	3.22	99.1

ZrC

The microstructure of the unirradiated ZrC is dominated by a large number of small black dots due to ion milling with 5 KeV Ar ions, Figure 2. Rel-rod dark field images did not reveal any faulted loops in the unirradiated ZrC. Bubbles approximately ~1 nanometer in diameter were identified using overfocus (shown as black dots) and underfocus (shown as white dots) imaging technique. These small bubbles are believed to be due to damage caused by ion milling with argon ions. No precipitates were found in the unirradiated ZrC. The ZrC before irradiation has a FCC structure with a measured lattice constant of 0.471 nm, consistent with the data of 0.473 nm in literature [12]. The Kikuchi line patterns due to the inelastic scattering of electrons from atomic planes are clearly visible under convergent beam diffraction. A few scattered voids and line dislocations were found at low magnification. No ring pattern was identified under select aperture diffraction (SAD).

For the ZrC sample irradiated at 800ºC to 10 dpa , a ring pattern developed in the diffraction pattern, Figure 3(a). The measurement from the diffraction spots from zone [011] revealed a 0.6% increase in lattice constant. No voids or faulted loops are identified in the 10-dpa sample. The irradiated microstructure of ZrC at a dose of 70 dpa is shown in Figure 3(b). The visibility

of the ring pattern increases while the visibility of Kikuchi pattern drops to nearly zero. However, the diffraction spots are still well defined when a small select-area aperture is used (~250 nm). The weak beam dark field image using the diffraction from ring indicated the ring pattern formed due to clusters approximately 50 nm in size. EDS measurement of these clusters shows similar chemical composition to ZrC. No voids, faulted loops or amorphization were identified. However, few cracks along the grain boundaries were identified. The measurement of lattice constant from the diffraction pattern at zone [011] indicated an approximately ~ 7% increase compared to the unirradiated ZrC, Figure 4. The spot shape of the diffracted beam in the diffraction is severely deformed comparing to the unirradiated or low dose samples.

ZrN

The microstructure of the unirradiated ZrN is shown in Figure 5 (left) with clear evidence of ion milling damage. There are a few areas with precipitates, scattered voids and dislocation lines, shown in Figure 5 (right). EDS revealed the circular shaped precipitates (typically < 200 nm) are rich in Zr and O and believed to be ZrO_2. A few large polygon shaped precipitates (typically > 1 µm) at grain boundaries are also observed. These precipitates are rich in Al and O with an atomic ration near 2:3 and are likely Al_2O_3. The diffraction pattern and Kikuchi line pattern for the unirradiated ZrN is clear despite the defects caused by ion milling damage.

The microstructure of ZrN irradiated to 10 and 70 dpa at 800ºC is shown in Figure 6. No dislocation loops (faulted or perfect) were identified. Moiré fringes were found in many areas of the sample, Figure 6 (a) and (b). EDS measurements indicate the areas with Moiré fringes are rich in Zr, N and O. Bubbles are clearly visible in the under or over focus imaging condition shown in Figure 6 (a). Diffraction pattern from the large Al_2O_3 precipitates indicate the precipitates became fully amorphous at 70 dpa. No amorphization in ZrN was found. Similar to the 70 dpa ZrC sample, the visibility of Kikuchi pattern drops to zero. However, the select area diffraction at major zones still show clear FCC diffraction spots with high index spots elongated at a large aperture size (~1.25 µm). Comparison of the diffraction pattern from major zone [011] and [001] is shown in Figure 7. The change in the lattice constant is clearly visible with an increase of approximately ~ 9%. Different from ZrC, there are extra spots shown in both diffraction patterns at zone [011] and [001], suggesting an ordered FCC structure may be formed by irradiation.

TiC

Similar to ZrC, the microstructure of the unirradiated TiC shows uniformly distributed small defect clusters, shown in Figure 8. The microstructure appeared relatively clean, no evidence of precipitates or line dislocations was observed in contrast to the unirradiated ZrC and ZrN. Diffraction spots and Kikuchi patterns are clearly visible showing a well defined FCC structure. There were a few areas showing scattered cavities. At a dose of 10 dpa, small dislocation loops and dislocation segments are observed, shown in Figure 9. For the TiC irradiated to 70 dpa at 800°C, the microstructure consists of dislocations, loops and voids, shown in Figure 10. Weak beam dark field images (Figure 10, center) give a better view of dislocation loops and dislocation

network. These loops appear to be perfect loops with a Burgers vector of the $(a_0/2)[011]$ type.
No faulted loops were identified at 70 dpa. Voids were measured with an average size of 5.5 nm
at a density of 1.1×10^{15} cm^{-3}. The calculated void swelling at 70 dpa is approximately 0.01%.

No evidence of radiation induced precipitates or amorphization in TiC matrix are found. There
are no noticeable changes in the Kikuchi patterns after irradiation up to 70 dpa. A comparison of
diffraction spots from the major zone [001] and [011] between the unirradiated and the 70-dpa
sample is shown in Figure 11, indicating only a minor change in the spacing of the diffraction
spots. The measurement on the diffraction spots indicates a lattice increase by approximately ~
2% in the TiC irradiated to 70 dpa at 800°C.

TiN

The unirradiated microstructure of TiN is shown in Figure 12. Both images were taken with
<200> diffraction, showing defect clusters with a few scattered line dislocations. No evidence of
precipitates, amorphous phase, cavities and faulted loops was found. Kikuchi patterns were clear
in the areas with right foil thickness.

There is no 10-dpa irradiation condition for TiN. The irradiated microstructure for 70 dpa TiN is
dominated by dislocation lines and loops. The defect clusters shown in the unirradiated sample
are almost completely wiped out. Figure 13 shows dislocations from the same area under
different imaging condition, the <200> diffraction at bright field (left), weak beam dark field at
<200> diffraction (middle), and <0-22> diffraction (right). Similar to TiC, these loops are
perfect loops with a Burgers vector of the $(a_0/2)[011]$ type. The estimated loop size and density
is 17 nm and 3×10^{15} cm^{-3}, respectively. Evidence of radiation induced precipitates, voids, faulted
loops, and amorphization are not found. Similar to TiC, the Kikuchi patterns in the irradiated
sample are clear even at 70 dpa. The comparison of diffraction patterns before and after
irradiation to 70 dpa is similar to TiC shown in Figure 11. The measured lattice increase for TiN
at 70 dpa is approximately ~ 2%.

SiC

For the hexagonal SiC there are many possible configurations due to the variation in its stacking
sequence along [0001] crystal direction. The microstructural analysis for the unirradiated SiC
indicates the SiC in this work is a 6H-SiC. Figure 14 provides the information on atomic
configuration for 6H-SiC. The unirradiated microstructure for SiC is shown in Figure 15. Most
of the areas on the sample show a uniform matrix with little evidence of ion milling damage
from sample preparation in contrast to the unirradiated ZrC, ZrN, TiC and TiN. Dislocations and
stacking faults are the main features can be found in the unirradiated SiC (See Figure 15, pictures
on the top). Due to large lattice constant (c=1.5117 nm), the projection of basal planes at edge-
on condition is clearly visible when imaged at zone [1,-2,1,0] without using the objective
aperture, shown in Figure 15. A close look at stacking faults reveals the spacing variation
between the fringes due to stacking faults on basal plane, Figure 16.

Although the JEOL2010 microscope with a LaB$_6$ filament is not set for high resolution TEM to reveal the atomic configuration, it still can be used to provide fine details of the 6H-SiC on its atomic layers along the [0001] direction. This is evidenced by the fine details present in Figure 17, where the fine line structure inside the major fringe corresponds to the 6 layers in 6H-SiC. If no stacking fault involved, there should be 6 fine lines between any two neighboring major fringes formed due to basal planes.

For the SiC irradiated to 10 dpa at 800°C, no evidence of radiation induced microstructural changes can be identified. Both diffraction and Kikuchi patterns look no different compared to the unirradiated SiC. Similar to the unirradiated case, stacking faults are still the main defect features present in the SiC matrix in the 10 dpa SiC, shown in Figure 18 (top). A close look at a crack at grain boundary triple junction is shown in Figure 18 (bottom). The matrix does not show any visible evidence of the radiation damage.

At the dose of 70 dpa, the irradiated SiC shows well developed dislocation loops, shown in Figure 19. These loops are imaged with a two-beam condition at diffraction of g=[2,-1,6] near zone [0,-1,1,0]. The picture on the right is a closer look of the same area shown on the left. The average loop size and loop density are measured to be 8.5 ± 2.7 nm and 4.7x10^{15} cm^{-3}, respectively. The loop size distribution is shown in Figure 20 where the largest loops have sizes up to 22 nm. The comparison of the diffraction patterns from major zones are shown in Figure 21. No noticeable degradation and spacing changes can be identified. There are small bubbles identified in both 10 dpa and 70 dpa samples, with the later one has a higher number density, shown in Figure 22. The quantitative characterization for the small bubbles are not attempted due to the small size (< 2 nm) and high density.

Discussion:

ZrC

The sample irradiated at 800°C to 70 dpa resulted in a significant increase of 7% in lattice constant comparing to the unirradiated ZrC matrix. It is difficult to believe the 7% increase in lattice constant resulted from point defect agglomeration. One assumption is that there were two parallel processes occurring during irradiation. One was radiation induced defect accumulation leading to a small increase in lattice expansion and the other was radiation-induced precipitation resulting in a fcc ZrC with a lattice constant approximately 7% greater than the unirradiated ZrC matrix. The binary phase diagram shows ZrC at 800°C or below will precipitate out α−Zr phase when C is below 38at% and precipitate out C when C is greater than 50at% [13]. It appears the original ZrC grain (> 5 μm), after irradiation to 70 dpa, consisted many small ZrC clusters (<50 nm) with crystal orientation deviated slightly from each other, shown in Figure 3. That suggests the precipitation could be the major contribution to the 7% increase in lattice expansion. The visibility of Kikuchi may be used as a signature to qualitatively evaluate the damage on crystal structure. The lack of Kikuchi lines in convergent beam diffraction at the proper foil thickness indicates a severe distortion of atomic planes.

An increase of 7% in lattice constant could result in a significant increase in volume and internal stress thus setting the condition for cracking along grain boundaries in thin areas. This could be part of the reason for grain boundary cracking although thermal stresses in the thin TEM foil may also contribute to grain boundary cracking. Due to severe displacement damage at 70 dpa, the fraction of defects occupying the interstitial sites may be significant. Unfortunately the measurement of volumetric change due to Kr ion irradiation was not feasible. The large ratio of surface area to volume in TEM foil may allow a large lattice expansion than in the bulk material by irradiation to a high dose.

The bubbles in the ZrC caused by ion milling did not grow into micro voids. The lack of micro voids in the irradiated ZrC suggests the material is resistant to void swelling. The lack of faulted loops indicates that ZrC responded differently to radiation than fcc metals. Irradiation produces point defects and defect clusters in the material. The evolution of these defects and clusters under radiation-enhanced diffusion, plus the interactions of these defects with various sinks, determines the irradiated microstructure. Unlike the fcc metals, the crystal structure of ZrC can be envisioned as a fcc lattice of Zr with C filling in the octahedral interstitial sites. According to the work by Li [14] on the inter atomic potential of ZrC, the properties of ZrC are dominated by the strong covalent bonds and the weak ionic bonds (Zr-C) and the original metallic bonds (Zr-Zr) can be neglected. The strong covalent bonding between Zr and C, plus the occupying of the octahedral interstitial sites in fcc Zr by C atoms, make the ZrC respond differently to irradiation than a typical fcc metals. It is possible that this unique structure and strong chemical bonding may significantly slow down the diffusion and increase the formation energy for both voids and faulted loops.

ZrN

The irradiated microstructure for ZrN is quite different from ZrC, for example the presence of Moiré fringes, the ordered structure, and the lack of ring patterns in diffraction. Moiré fringes were found on many areas of the irradiated ZrN even at 10 dpa. It is well known that Moiré fringes are due to the overlap of two crystals. Since area with Moiré fringes measured rich in Zr, N and O, it is assumed ZrO_2 film was formed during irradiation. The oxygen to form ZrO_2 may come from large polygon shaped Al_2O_3 precipitates found in the ZrN. Due to the wide spread of Moiré fringes, it is difficult to believe that the ZrO_2 precipitates pre-existed in the matrix produce the fringes. The amorphization of Al_2O_3 by irradiation indicates ZrN is much more stable under irradiation than Al_2O_3.

The diffraction patterns from zone [001] and [011] of the 70-dpa ZrN revealed a structure typically seen in an ordered fcc structure ($L1_2$). Structure $L1_2$ is a stable ordered fcc structure normally observed for a binary system like B_3A, such as Gu_3Au [15]. However, that arrangement requires atom A and B to share a common fcc structure. In the case of ZrN, it is a NaCl type structure with two sets of fcc structure overlapping, one from Zr atoms and the other from N atoms. The atomic ratio between two atoms in B_3A is also significantly different than that in ZrN. Therefore, the $L1_2$ ordered structure could not be used to explain the extra diffraction spots in ZrN irradiated to 70 dpa. It is assumed that the observed structure ordering is caused by the Zr atoms since its atomic scattering factor for electron is approximately 4 times of that for N

atoms. Another possibility is that the ordered structure may be due to ordering of interstitial or vacancy Zr atoms in the irradiated ZrN. The exact cause for the observed diffraction patterns in the 70 dpa ZrN can not be confirmed. The details and the mechanism of ordering for Zr atoms in ZrN under Kr irradiation are beyond the scope of this work.

Similar to ZrC, a large increase of approximately ~ 9% in the lattice constant was observed, shown in Figure 7. It may be assumed that a significant fraction of Zr atoms are in interstitial sites. The lack of Kikuchi patterns at 70 dpa indicates a severe distortion of the atomic planes. The lack of bubble growth and void formation may be partially due to the large fraction of interstitial Zr atoms that increase the internal stress in compression and the energy required for cavity development.

TiC & TiN

Microstructure changes due to Kr ion irradiation at 800°C for titanium carbide and nitride are relatively simpler than zirconium carbide and nitride. The obvious difference is the evolution of the dislocation loops by irradiation. Although TiN has significant fraction of porosity as revealed by SEM, observation in TEM indicated no cavity or voids in the matrix. The fraction of porosity in TiN shown in Figure 1 should have no effect on the microstructure evolution under Kr ion irradiation. Network dislocations and dislocation loops are observed in the irradiated TiC and TiN, but not in ZrC and ZrN. At a dose of 70 dpa, the change on the visibility of Kikuchi patterns is not obvious, indicating the radiation damage on atomic planes is minor.

The diffraction patterns of the unirradiated and the irradiated TiC and TiN to 70 dpa remained nearly the same. No radiation induced precipitates, ordering or amorphization are identified at a dose of 70 dpa. It appears that the development of dislocations and loops is beneficial for TiC and TiN leading to more stable microstructures under Kr ion irradiation than ZrC and ZrN. Since the dislocation loops are identified as perfect loops, their contribution to mechanical property degradation at high temperature is expected to be minor. Also these loops and dislocations could be beneficial at high temperature by improving the ductility due to the presence of mobile dislocations. Although voids are present in the irradiated TiC, its contribution on swelling is negligible (~0.01% at 70 dpa). Besides the radiation induced dislocation network and loops, the main damage from irradiation is still an increase in lattice spacing of approximately ~ 2% for TiC and TiN.

SiC

The microstructure characterization for both unirradiated and irradiated 6H-SiC suggests that SiC has the least radiation damage than the other 4 ceramics which are all in fcc structure. The lack of evidence from ion milling damage for the unrradiated sample is not expected since the other 4 ceramics all suffer certain degree of ion milling damage during sample preparation. SiC has the largest unit volume (0.1242 nm^3) lowest molecular weight (40.1) among the 5 ceramics and the smallest atomic size for Si comparing to Ti and Zr. These differences may be partially responsible for its good resistance to the ion milling damage.

Since SiC is a very hard materials, the dislocations in the unirradiated SiC are believed to be introduced during materials fabrication. The stacking faults in 6H-SiC is a common feature in microstructure for this materials. Although some details of the projection of atomic layers along [0001] direction are revealed, Figure 17, the high quality high resolution image with much more details on atomic arrangement can only be obtained using the high-resolution TEM microscope. Nevertheless, the fine details in Figure 16 and 17 still provide useful information such as the spacing variation caused by stacking faults.

The lack of irradiation induced microstructural changes in the 10-dpa SiC indicates the material is not just resistant to the ion milling damage with Ar ions, but also resistant to high energy heavy ions up to a dose of 10 dpa. At high dose of 70 dpa, the loops are well developed. The threshold dose for loop formation must be greater than 10 dpa. This is different from TiC where loops are identified at 10 dpa. The average loop size for SiC at 70 dpa is roughly half of the loop size in TiN at 70 dpa. According to the work by Persson [9], these loops are most likely interstitial loops residing on (0001) planes. From the picture in Figure 19, the loops appear all in the shape of circular discs. A detailed study on the loop evolution as a function of irradiation dose and temperature is required to fully understand its role on microstrural evolution in 6H-SiC. The role of the loops in 6H-SiC on the mechanical and thermal stability needs further investigation. Although loops developed in SiC, the lack of degradation in Kikuchi pattern in the convergent beam diffraction pattern indicates that the radiation damage on microstructure in SiC at 70 dpa is much less than in Zr and ZrN.

To summarize this work: Refractory ceramics of ZrC, ZrN, TiC and TiN were irradiated with 1 MeV Kr ions at 800°C to 70 dpa. Zirconium carbide and nitride developed severe microstructure damage evidenced by the disappearance of Kikuchi patterns and a significant increase in lattice constant (7- 9%). An ordered microstructure was developed in ZrN at 70 dpa. No voids were found in the irradiated ZrC, ZrN and TiN. The microstructure stability under Kr ion irradiation for SiC, TiC and TiN is significantly better than ZrC and ZrN as evidenced by no obvious degrdation in Kikuchi and diffraction patterns before and after irradiation and a smaller increase in lattice constant (~ 2%). Voids were only found in the irradiated TiC and the corresponding swelling is negligible (~0.01%). Dislocation networks and perfect loops were found in the irradiated TiC and TiN and are believed to be beneficial for microstructural stability under heavy ion irradiation. Dislocation loops are well developed in SiC at 70 dpa. Radiation-induced secondary-phase precipitates, amorphization are not found in the matrix of the carbides and nitrides. The cubic structure ceramics investigated in this work retain their fcc crystal structure at a dose of 70 dpa. 6H-SiC has been identified as the best on microstructural stability among 5 ceramics under Kr ion irradiation at 800°C.

Conclusion:

6H-SiC was identified to be the best among 5 ceramics on microstructure stability under Kr ion irradiation at 800°C. The radiation induced increase in lattice spacing in TiC and TiN is approximately ~ 4 times smaller than in ZrC and ZrN. It appears that among the 5 ceramics, the

one with lighter molecular weight performs better on the microstructure stability under heavy ion irradiation at 800ºC. Si or Ti atom is smaller and lighter than Zr atom, leading to a difference in the strength of the covalent bonds between SiC, TiC (or TiN) and ZrC (or ZrN) which may affect the recovery of radiation induced defects. The better microstructural performance of TiC over ZrC under Kr ion irradiation is consistent with the work on neutron irradiated TiC and ZrC at a low temperature and dose [6].

A follow-on neutron irradiation at 800°C using the advanced test reactor at the Idaho National Laboratory has been planned, but at a much lower does level (~ 1 dpa at 800ºC). However, a high dose neutron irradiation at high temperature will be needed to verify the results from this work. The Futurix_MI irradiation program between DOE and CEA will provide critical neutron irradiation data to the GFR materials program.

Note that heavy ion irradiation of TEM disc samples has its limits when simulating neutron irradiation effect in bulk materials. Care has to be taken when applying these results to evaluate the material microstructural changes under neutron irradiation in reactors. Before high dose data of fast flux neutron irradiation at high temperature become available, a follow on study on using proton irradiation for the same set of ceramics is recommended. This will provide an opportunity to verify the results in this work while offer a limited mechanical test capability to evaluate the radiation effects on the materials mechanical property changes.
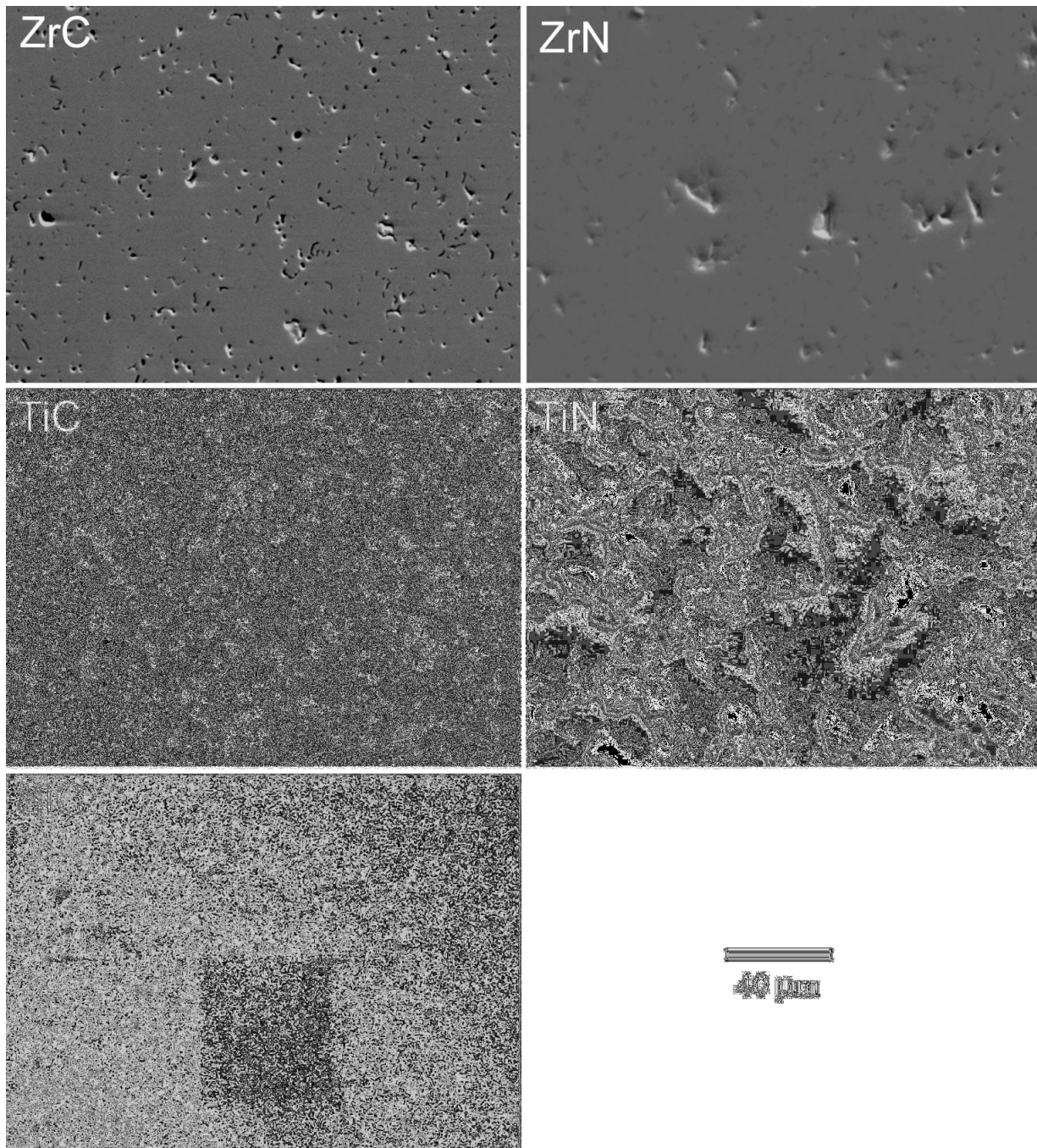
Figure 1. SEM images of the as-received ZrC, ZrN, TiC, TiN and SiC. The large fraction of porosity in TiN is consistent with its low relative density approximately 91% of the theoretic density.
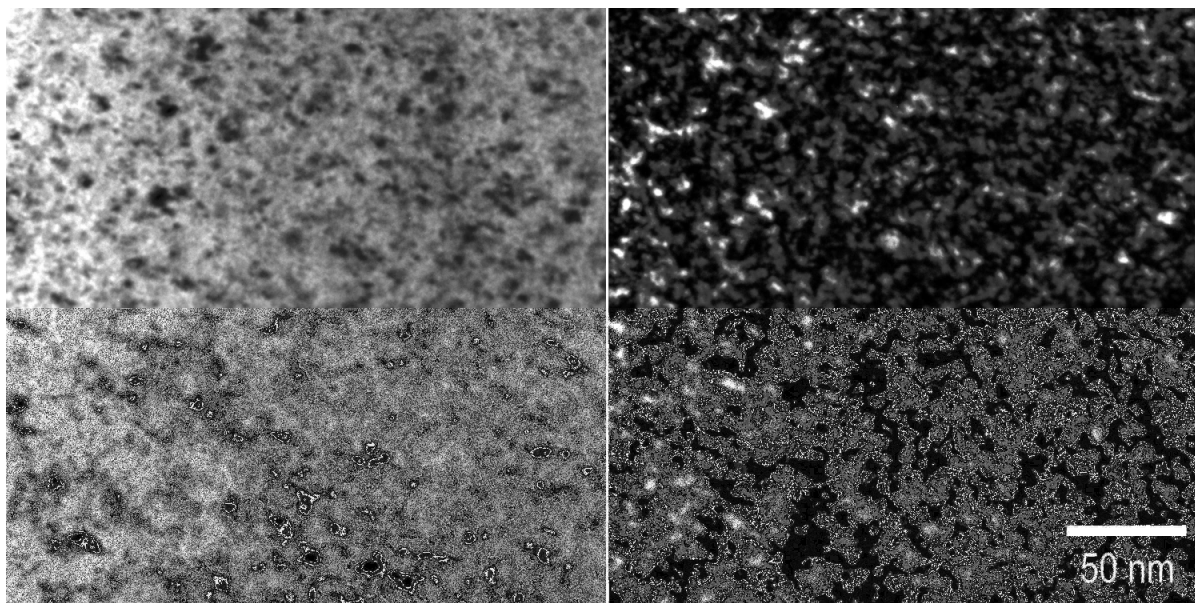
Figure 2. Microstructure of unirradiated ZrC imaged with **g**=200 near zone [011]. The left is bright field image and the right is weak beam dark field image pair showing black dot damage from ion milling.
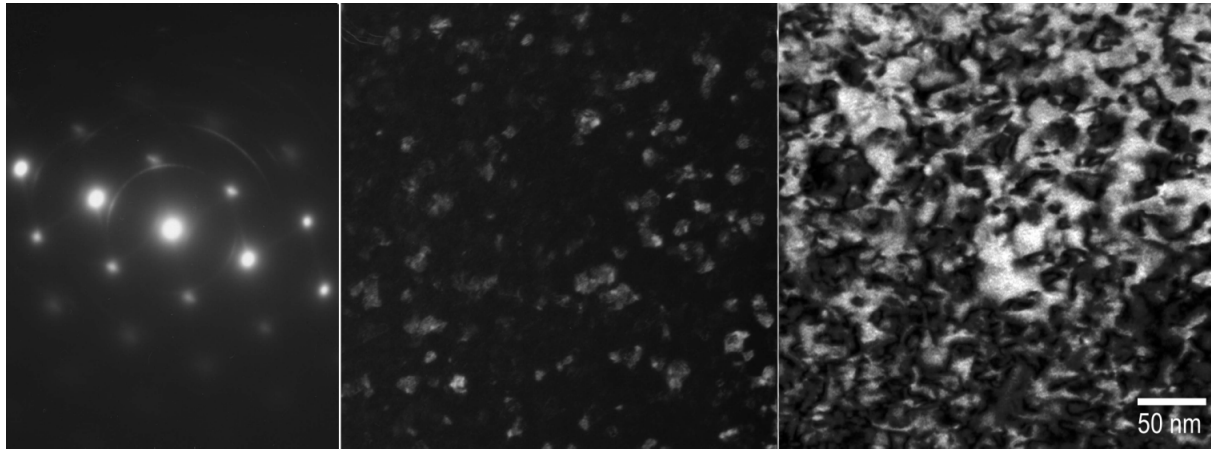
Figure 3a. ZrC irradiated at 800 ºC to 10 dpa, showing a ring pattern (left), the dark field image using the 1st ring in diffraction (middle) and a **g**=200 bright field image showing dislocations (right).
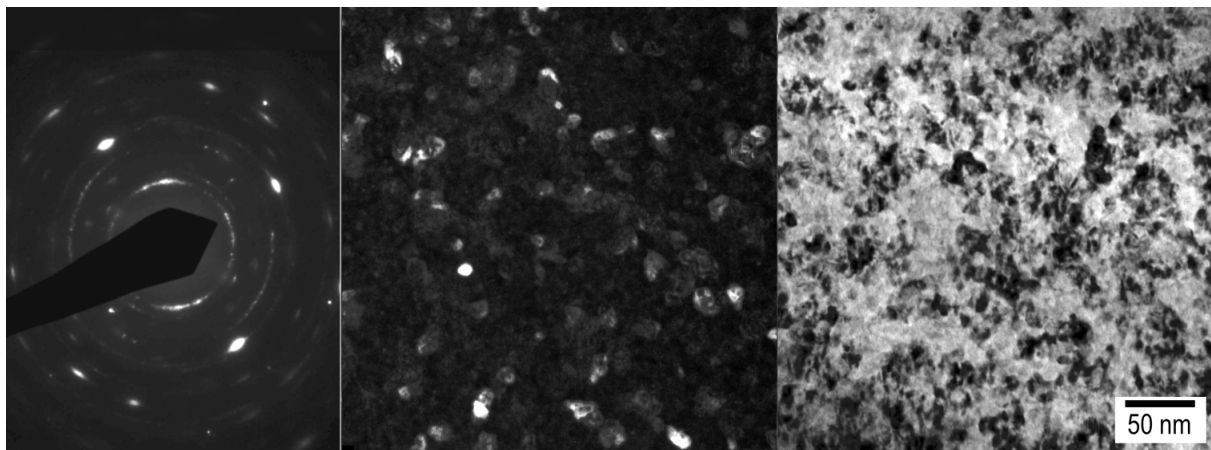
Figure 3b. ZrC irradiated at 800 ºC to 70 dpa, showing ring pattern (left), the dark field image of precipitates using <111> diffraction from the 1st ring (middle) and a **g**=200 bright field image showing dislocations (right).
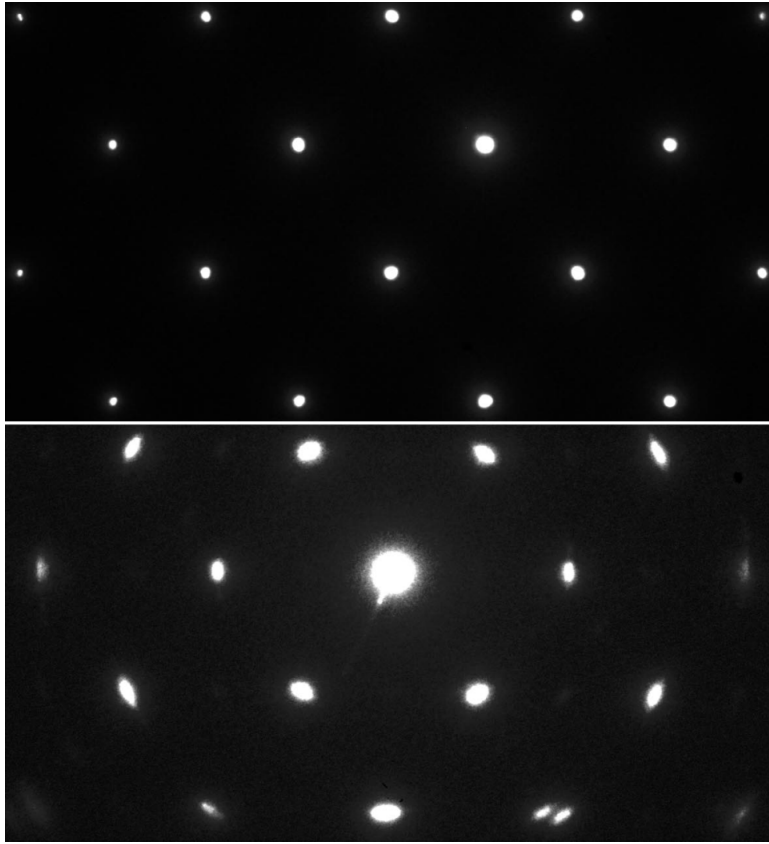
Figure 4. Selected area diffraction at zone [011] for ZrC, the unirradiated (top) and the irradiated to 70 dpa at 800°C (bottom) showing approximately 7% increase in lattice constant. Note that a shrink in the diffraction pattern spacing corresponds to an expansion in the real lattice space.
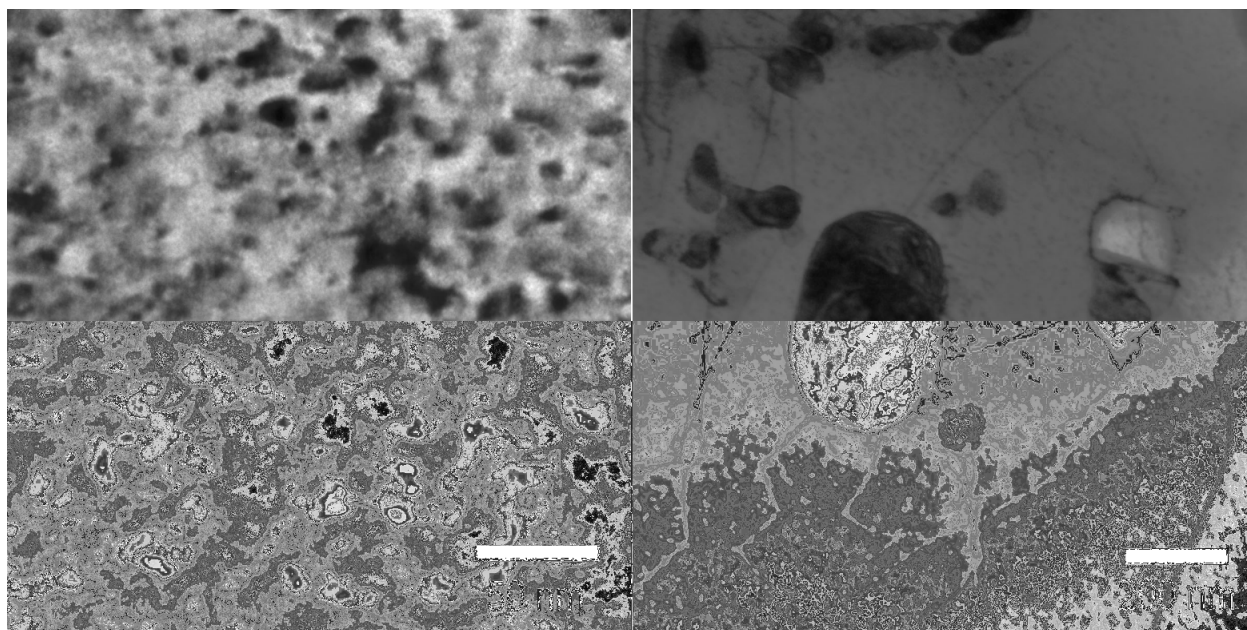
Figure 5. Microstructure of unirradiated ZrN imaged with **g**=200 near zone [011] (left) showing damage from ion milling. The low magnification on the right shows an area with dislocations, voids, Zr-O precipitates (dark precipitates) and the fine defect clusters.
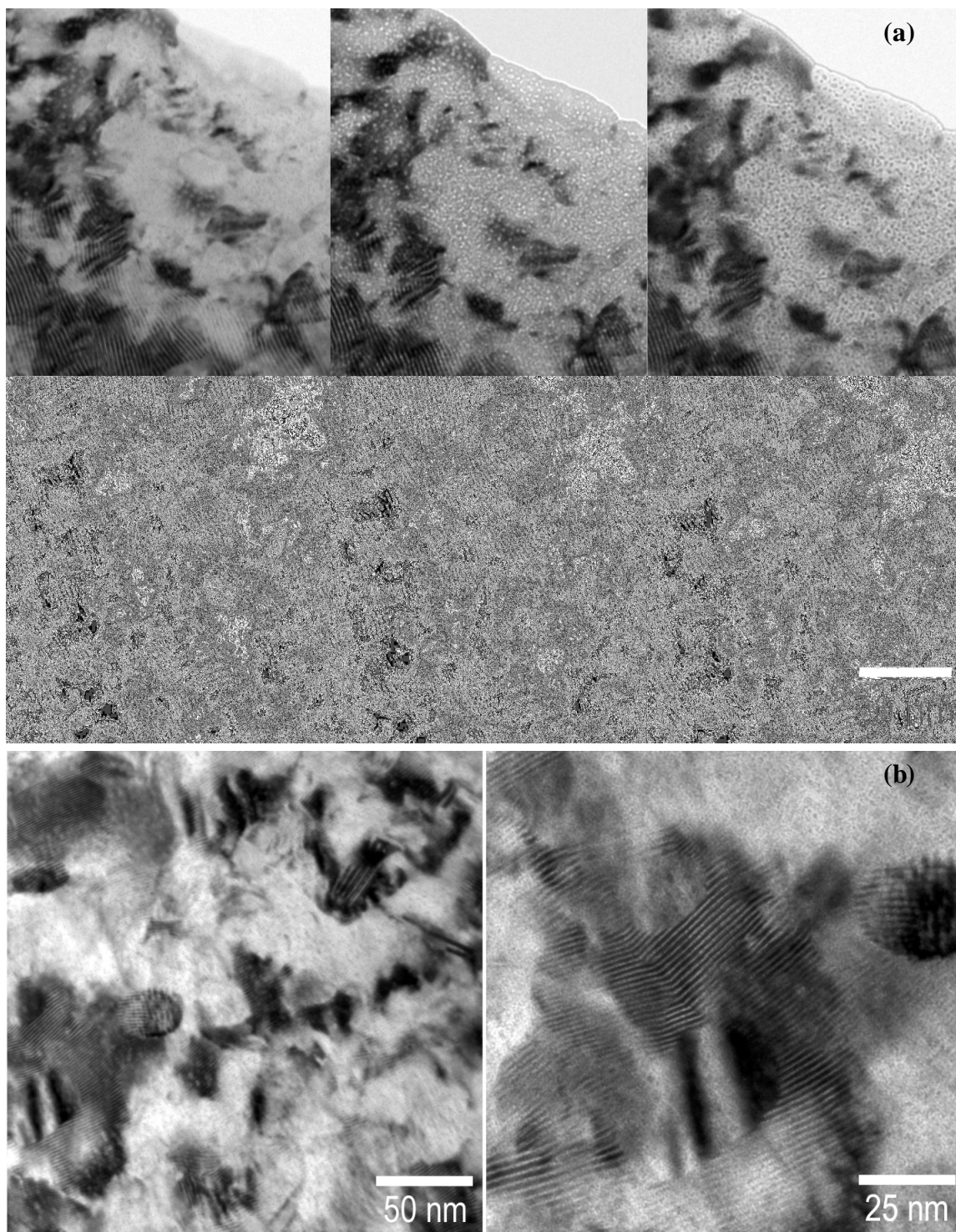
Figure 6. Microstructure of ZrN irradiated with 1 MeV Kr ions at 800ºC to (a) 10 dpa (top) and (b) 70 dpa (bottom) imaged with **g**=200 near zone [011] showing defect clusters with Moire patterns. The images on top (10 dpa) also reveal the bubbles in the under-focus (middle) and over-focus (right) imaging condition.
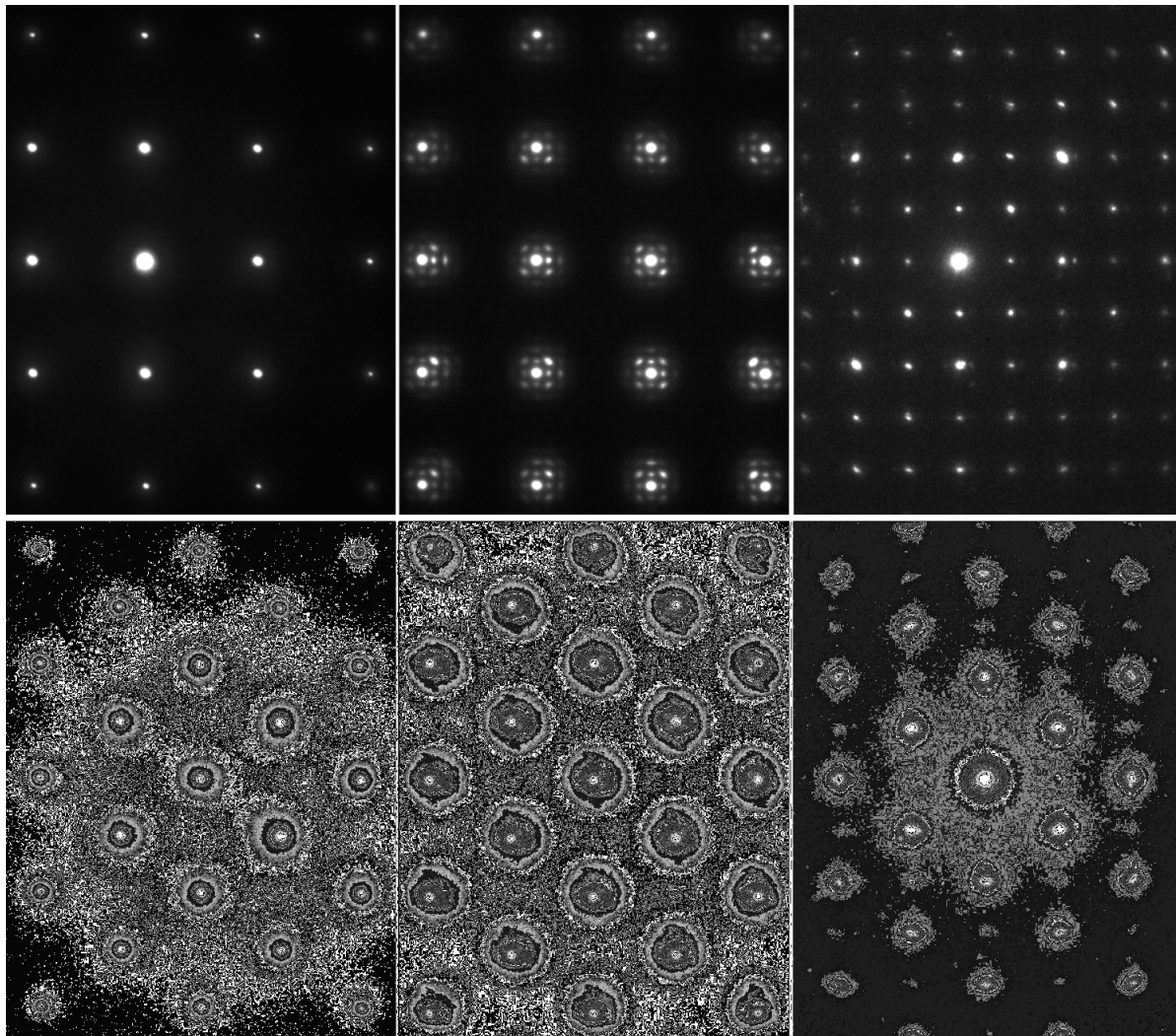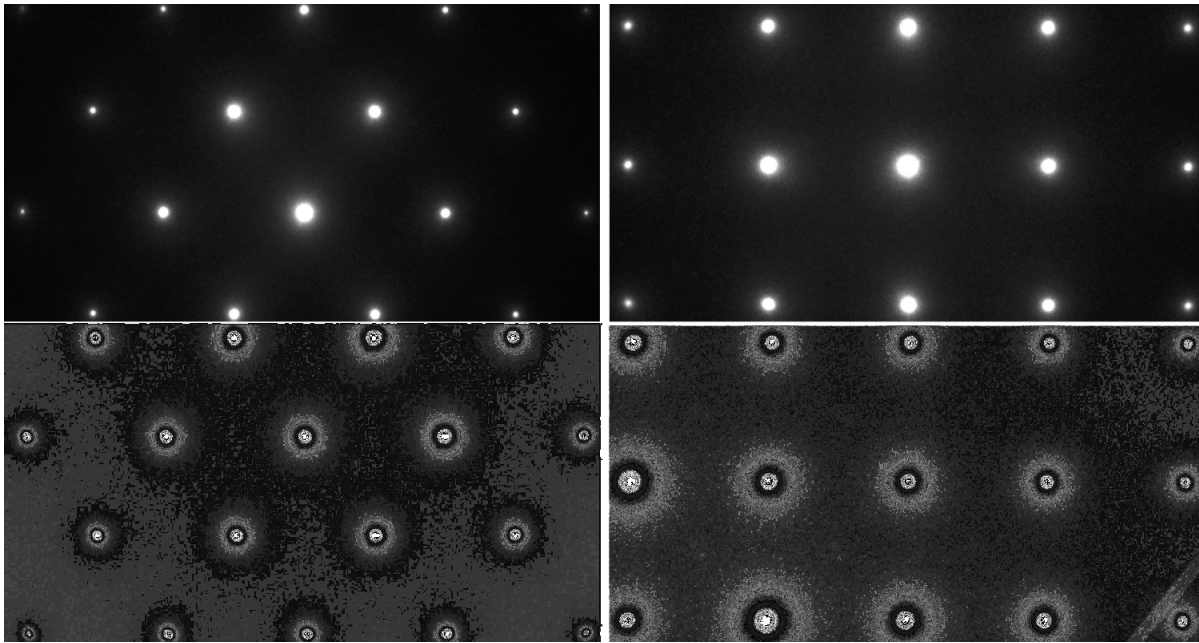
Figure 7. Comparison of diffraction patterns for ZrN at zone [011] (left) and [001] (right) between the unirradiated (top) and the irradiated (bottom) showing an ordered FCC (LI$_2$) structure and a lattice increase of ~ 9% due to irradiation. Captiopn should explain middle graphs also.
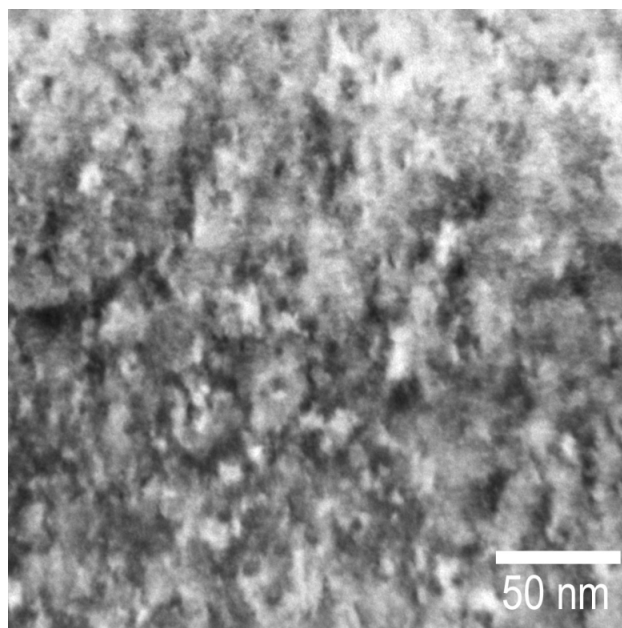
Figure 8. Microstructure of the unirradiated TiC imaged with **g**=200 showing defect clusters due to ion milling damage.
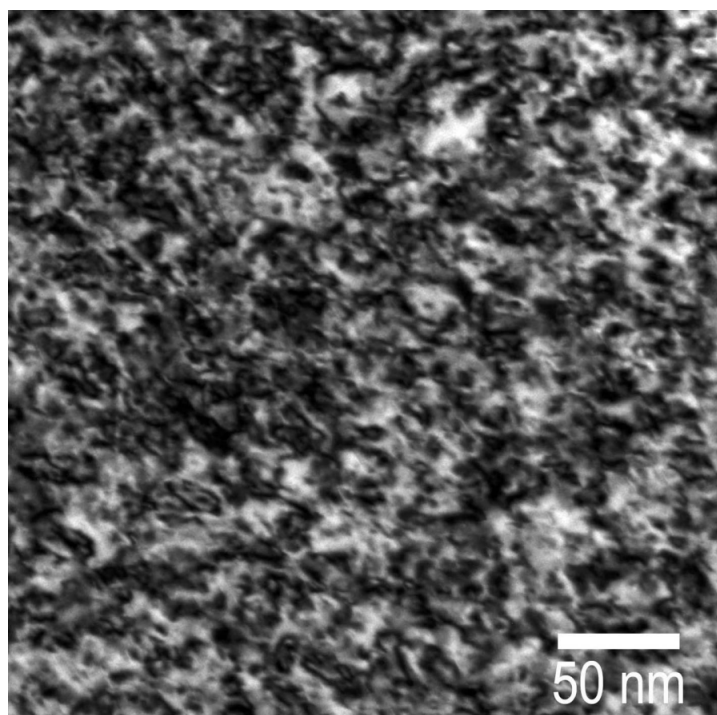
Figure 9. Microstructure of the 10-dpa irradiated TiC imaged with **g**=200 showing dislocation loops.
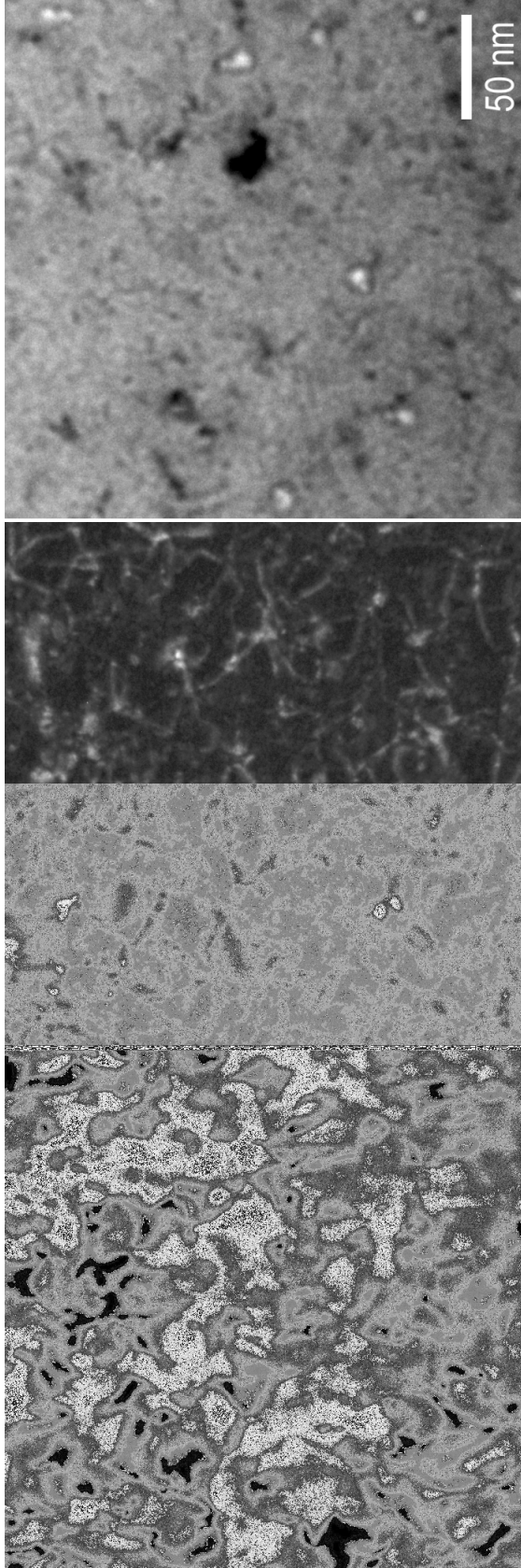
Figure 10. Microstructure of TiC irradiated with Kr ions to 70 dpa at 800°C (imaged with **g**=220) showing dislocations in bright field (left), weak beam dark field (3**g**) (middle) and voids (right).

Figure 11. Comparison of diffraction patterns for TiC at zone [011] (left) and [001] (right) between the unirradiated (top) and the irradiated to 70 dpa at 800°C (bottom) showing a lattice increase of ~2.4% due to irradiation.
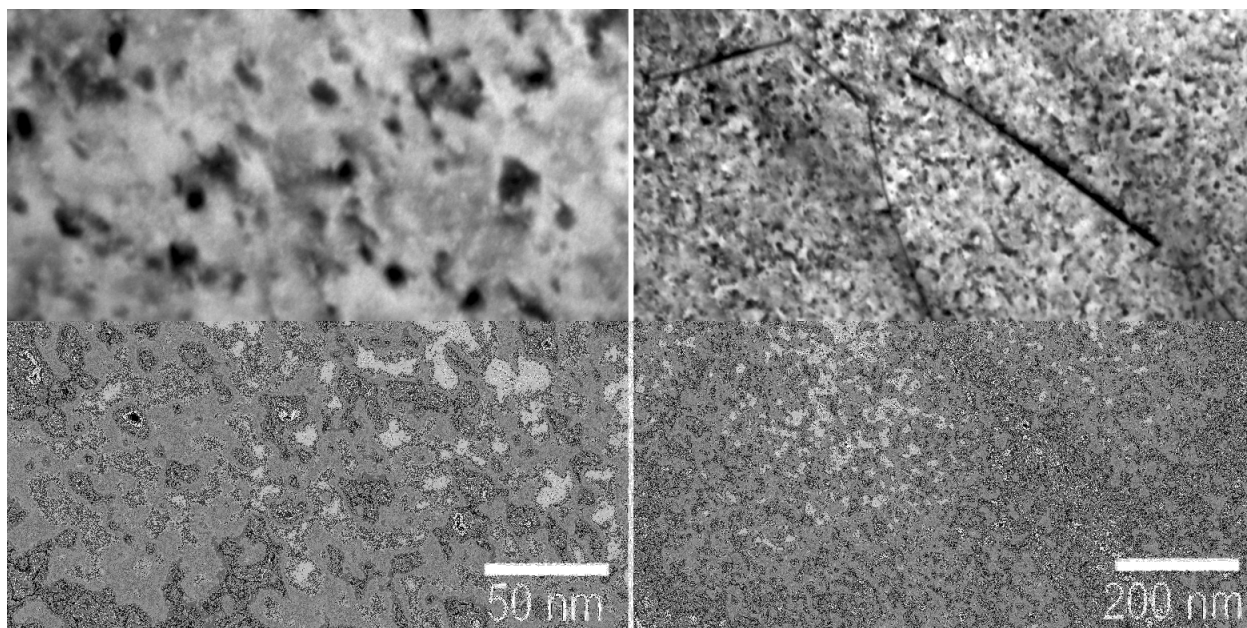
Figure 12. Microstructure of the unirradiated TiN imaged with **g**=200 showing defect clusters from ion milling damage (left) and dislocations at low magnification (right).
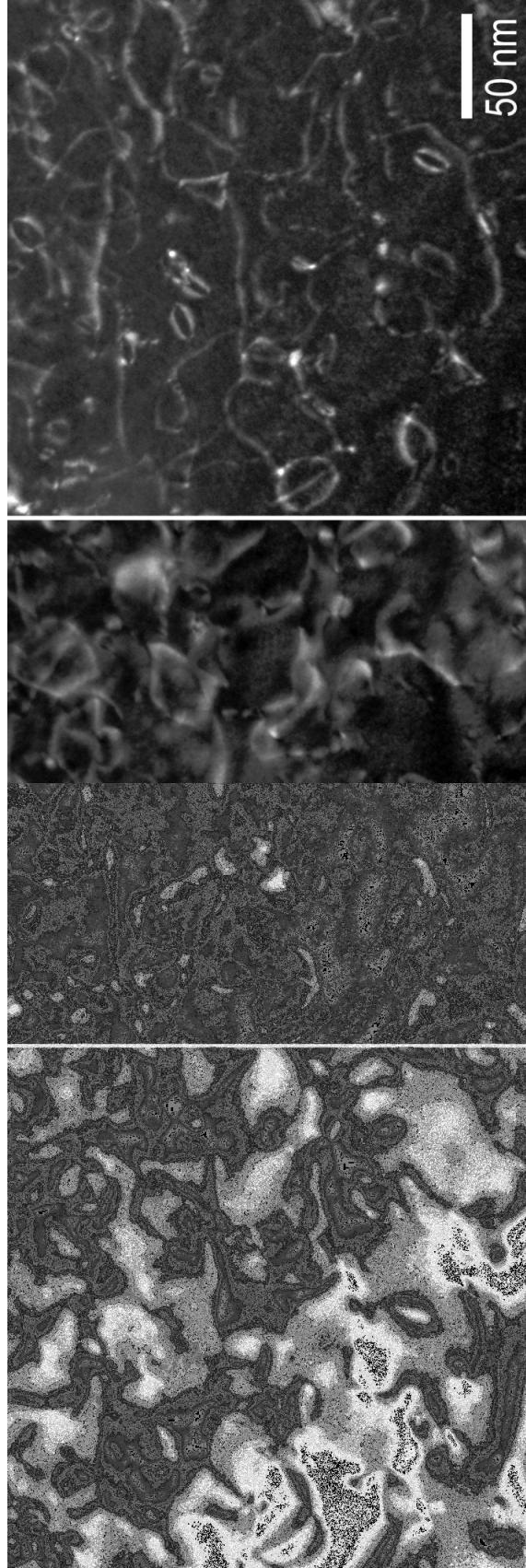
Figure 13. Microstructure of TiN irradiated with Kr ions to 70 dpa at 800°C showing dislocations in the same area imaged with **g**=200 bright field (left), weak beam dark field (middle) and with **g**=0-22 (right). The loops were identified with a Burgers vector of type $0.5a_0[011]$.
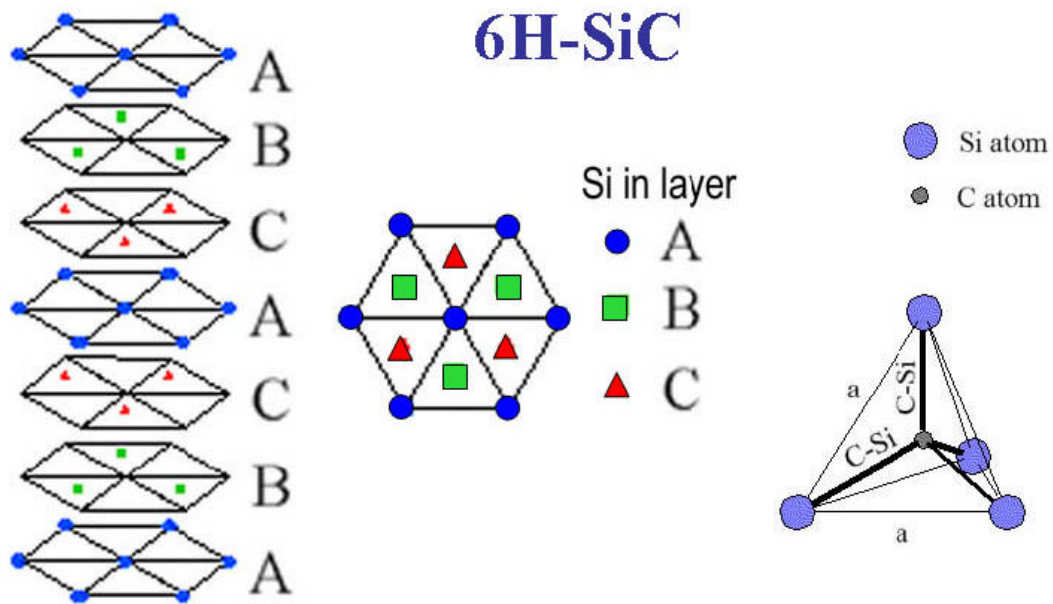
Figure 14. Crystal structure for 6H-SiC. It is a hexagonal with a = 0.30806 nm and c = 1.51173 nm. The stacking sequence repeats itself after every 6 layers of Si along the [0001] direction.
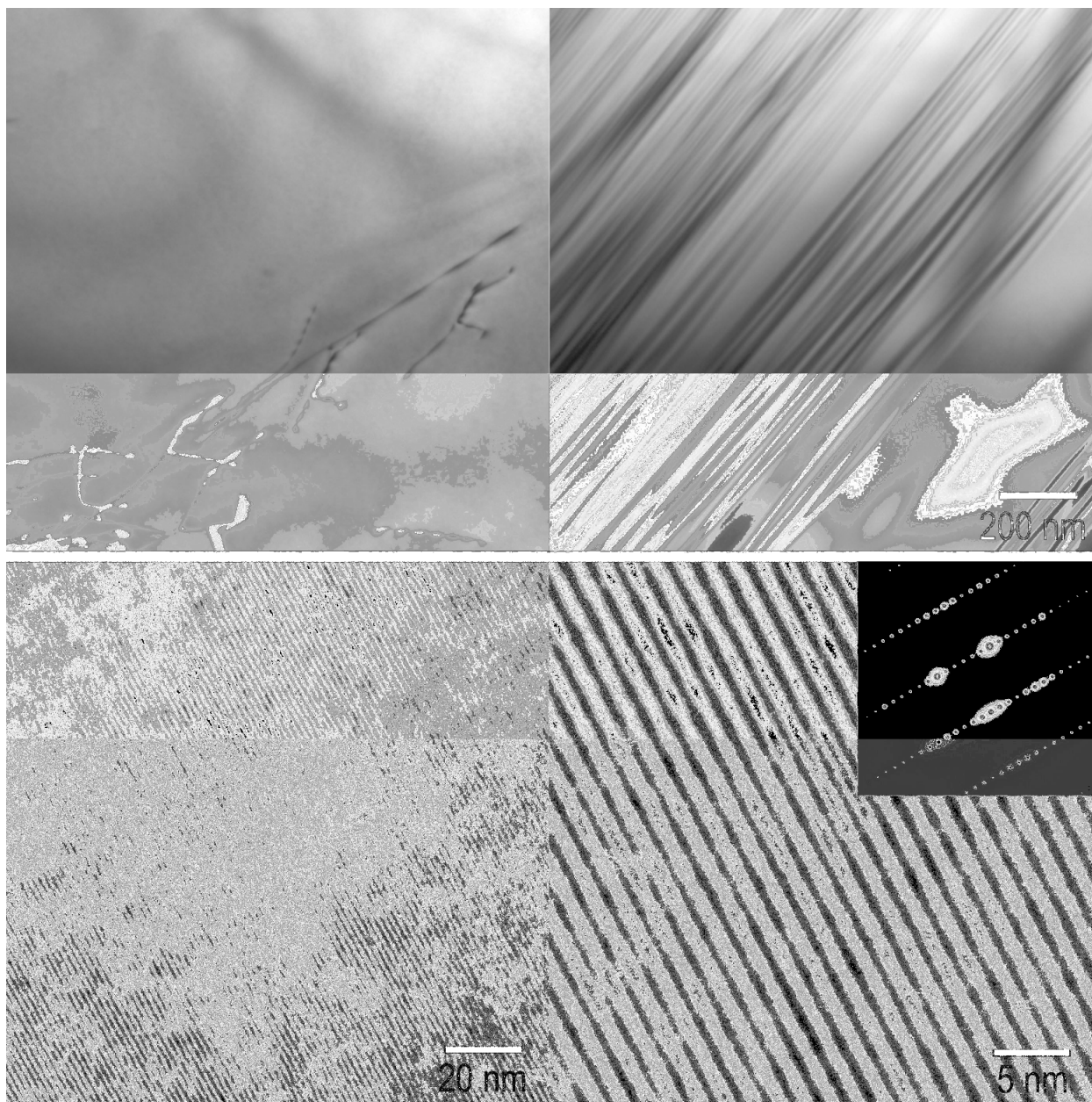
Figure 15. Microstructure of the unirradiated SiC. It shows scattered dislocations (top-left) and a group of stacking faults (top-right). The high resolution images (bottom) reveal the projection of basal planes at edge-on condition. The insert shows the diffraction at zone [hkil]=[1,-2,1,0] which is used to form the high resolution images.
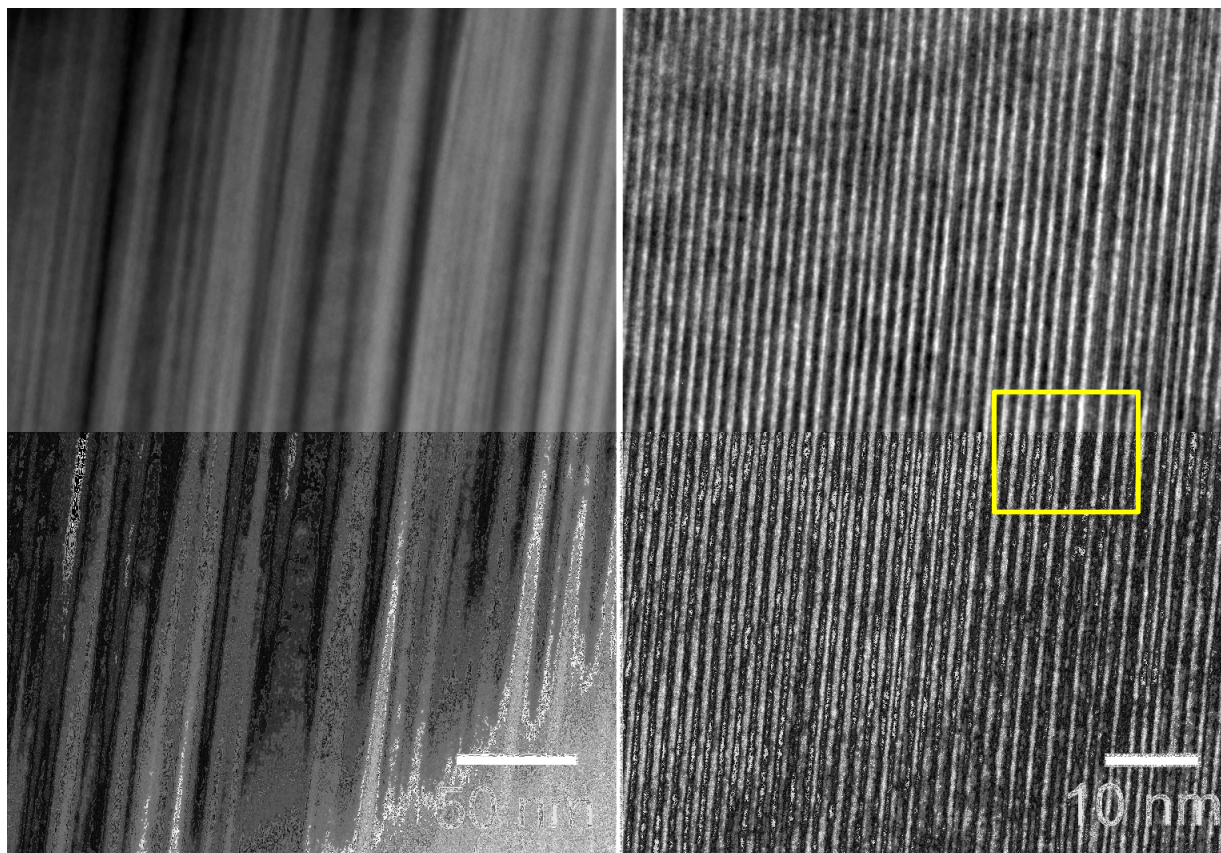
Figure 16. A close look at the details of the stacking faults. Note the spacing variation between the lines (projection of the basal planes) in the high resolution image (right) which reveals the stacking faults on basal planes.
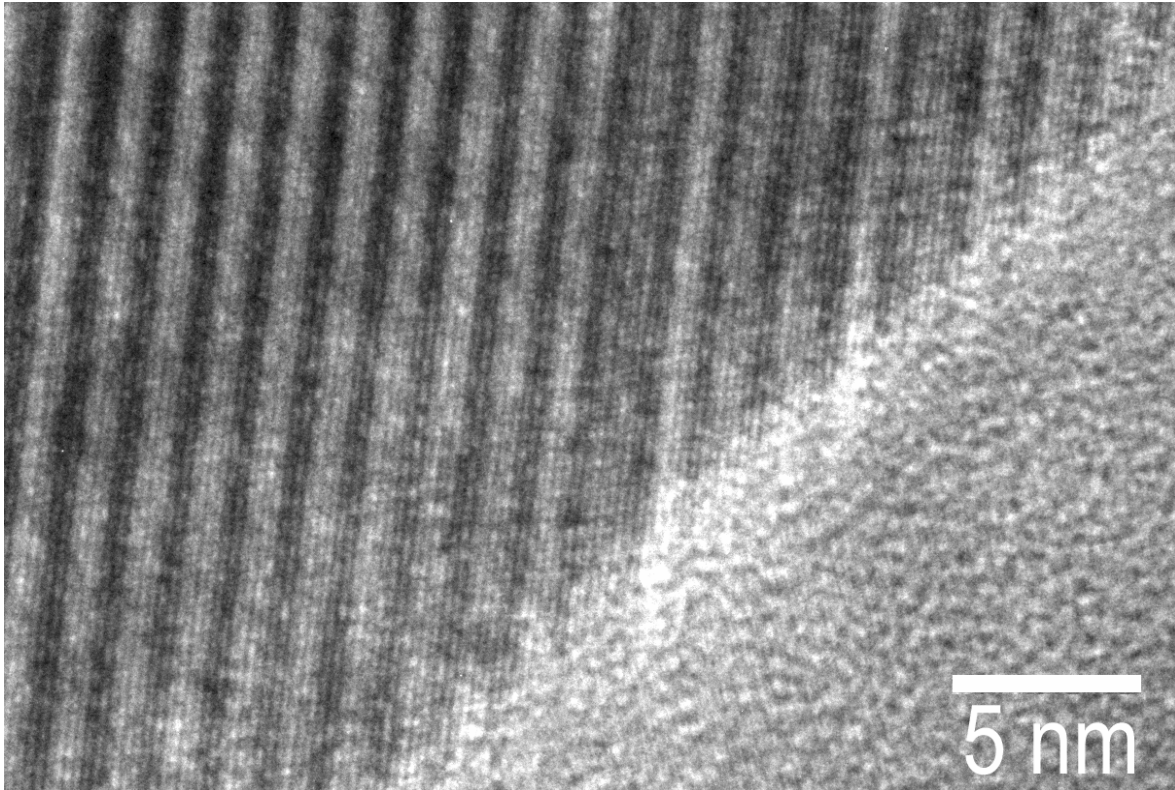
Figure 17. The details of the fine lines inside the major fringes in the picture correspond to 6 atomic layers in 6H-SiC. There are 6 fine lines between any two neighboring major fringes. The picture also shows a grain boundary.
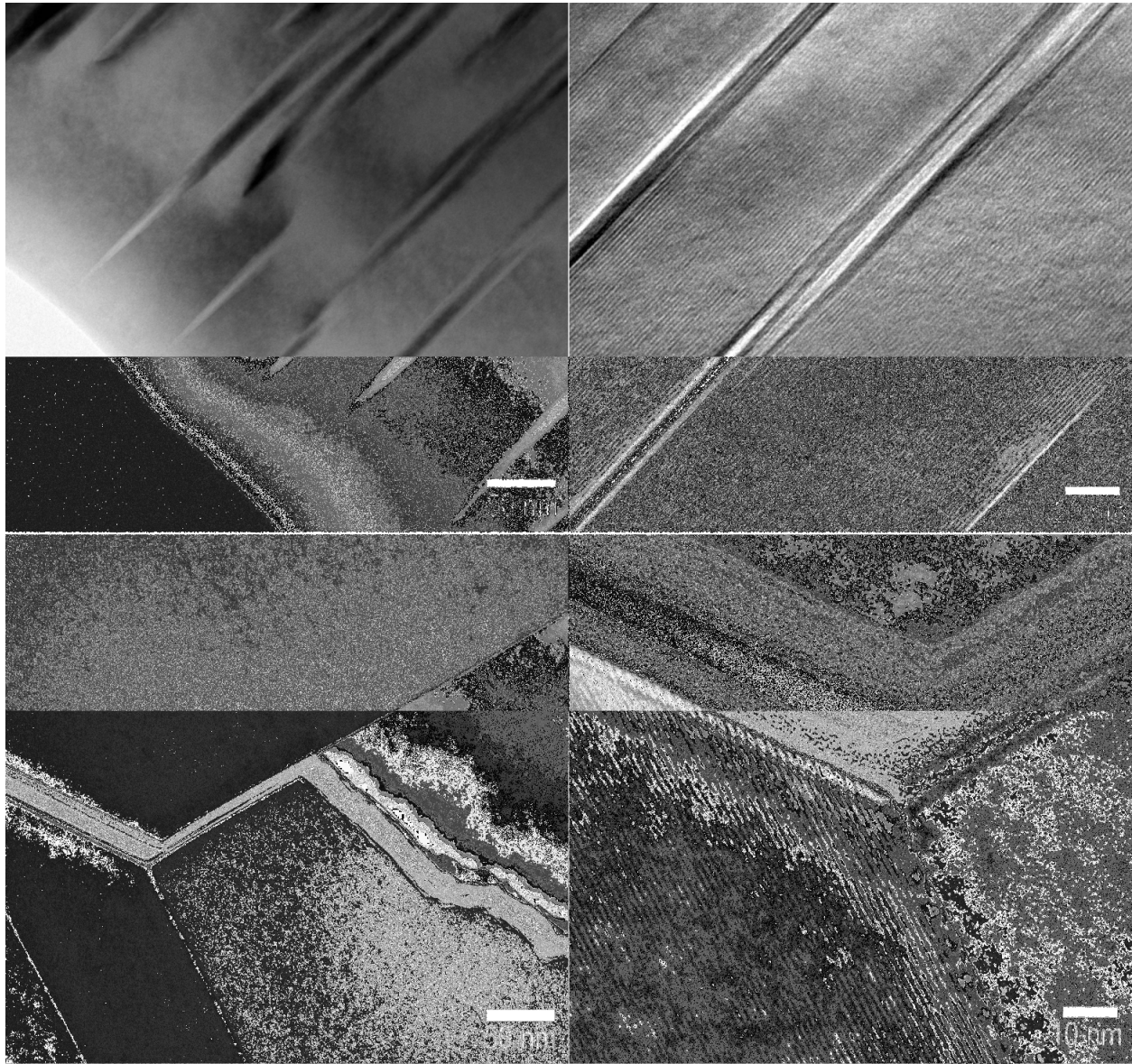
Figure 18. Microstructure of 6H-SiC irradiated with 1 MeV Kr ions to 10 dpa at a temperature of 800 ℃. Radiation induced defects are not visible at this dose. The picture on the top shows a group of stacking faults similar to the unirradiated sample condition. The picture on the bottom shows a fracture at grain boundary triple junction. Pictures on the right provide a detailed view of the same area shown on the left.
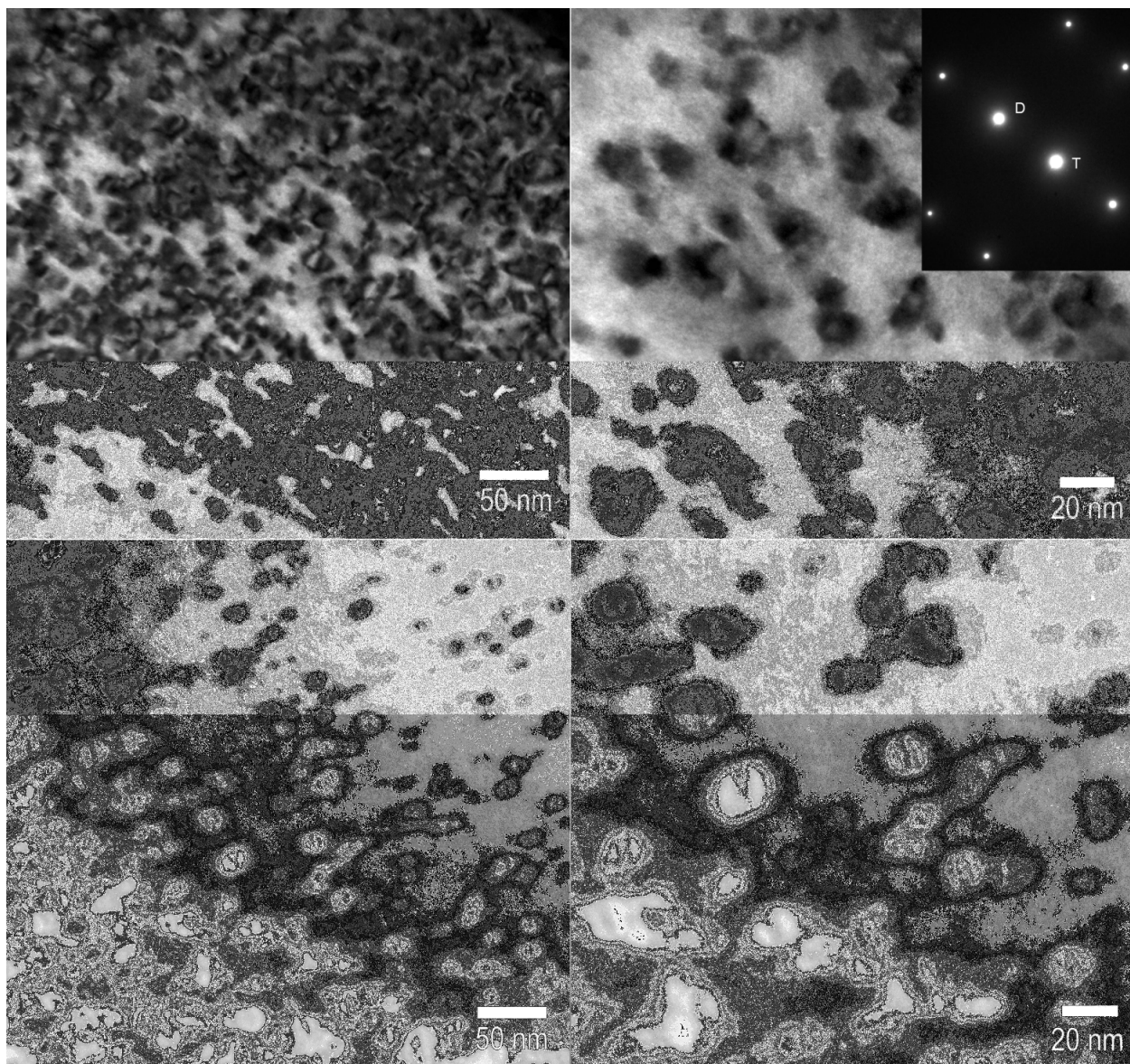
Figure 19. Microstructure of 6H-SiC irradiated with 1 MeV Kr ions to 70 dpa at a temperature of 800 ℃. Dislocation loops are imaged with g = [2,-1,6] and the exact diffraction condition for the loops in the pictures (top) is shown in the insert. The pictures on the right provide a detailed view of the same area shown on the left.
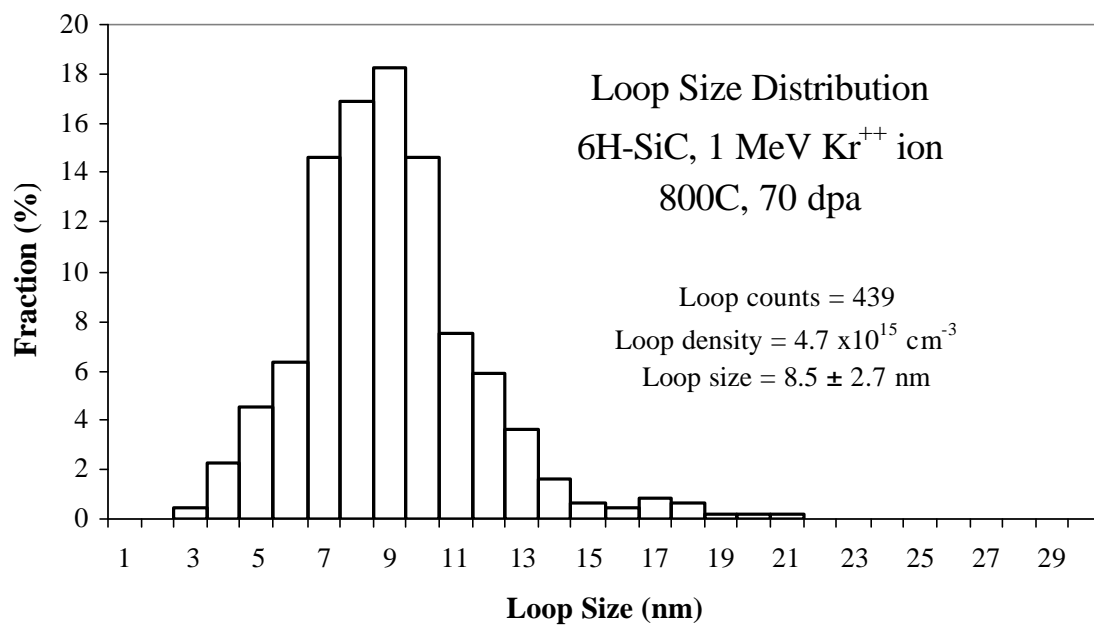
Loop Size Distribution

6H-SiC, 1 MeV Kr^{++} ion

800C, 70 dpa

Loop counts = 439
Loop density = 4.7 x10^{15} cm^{-3}
Loop size = 8.5 ± 2.7 nm

Fraction (%)

Loop Size (nm)

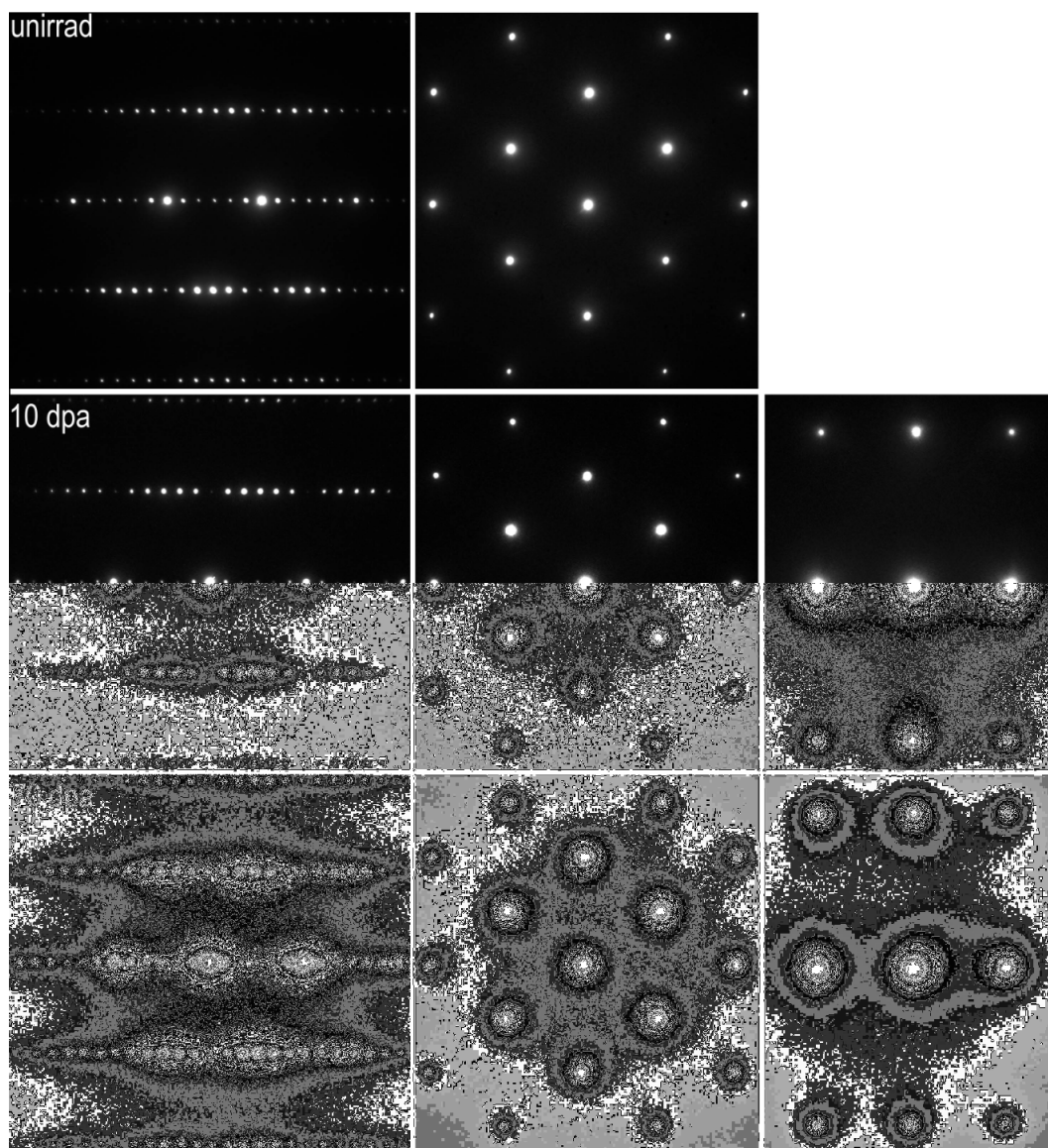Figure 20. Loop size distribution for 6H-SiC irradiated with 1 MeV Kr ions to 70 dpa at a temperature of 800 ℃.

Figure 21. Diffraction patterns from the major zone [1,-2,1,0] (left), [0,2,-2,-1] (middle) and [0,-1,1,0] (right), for 6H-SiC in the condition of the unirradiated (top), irradiated at 800ºC to dose of 10 dpa (middle) and 70 dpa (bottom) with 1 MeV Kr ions.
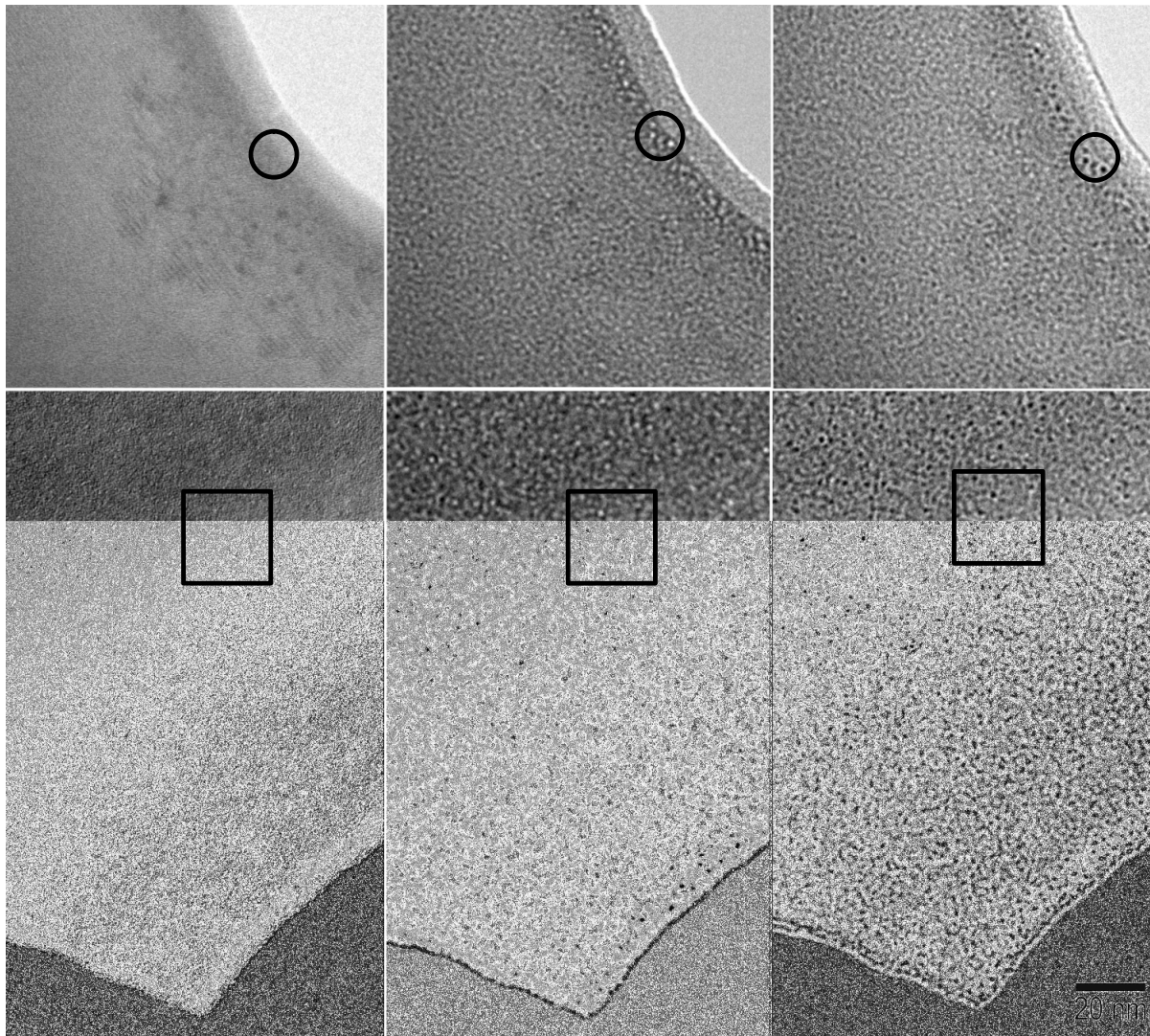
Figure 22. Small Bubbles (< 2 nm) in the 6H-SiC irradiated with 1 MeV Kr ions at 800ºC to 10 dpa (top) and 70 dpa (bottom) imaged under condition of in-focus (left), under-focus (middle) and over-focus (right). The density of bubbles is significantly higher in the 70 dpa sample. Small bubbles appear white and black dots with the under-focus and over-focus imaging condition, respectively.

Reference:

[1] L. W. Hobbs, F. W. Clinard, Jr., S. J. Zinkle and R. C. Ewing, J. Nucl. Mater., 216 (1994) 291

[2] Minato, K., et al., 1997, J. Nucl. Mater. Vol. 249, pp 142-149.

[3] Andrievskii, R., et al., 1978, Izv. Akad. Nauk SSSR, Neorg. Mater. Vol. 14, pp 680-83.

[4] Kovalchenko, M., Rogovoi, Y., 1973, Izv. Akad. Nauk SSSR, Neorg. Mater. Vol. 9, pp 321-22

[5] G.W. Keilholtz, R.E. Moore, and M.F. Osborne, Nuclear Application, 4 (1968) 330

[6] D. A. Dyslin, R. E. Moore and H. E. Robertson, ORNL-4480 (1969) p245

[7] W. J. Weber, L. M. Wang and N. Yu, Nucl. Instr. Methods in Phys. Research B., 116 (1996) 322

[8] P. O. A. Persson, L. Hultman, M.S. janson and A. Hallen, R. Yakimova,, Journal of Applied Physics, V. 93, #5, (2003) 9395

[9] P. O. A. Persson, L. Hultman, M.S. janson and A. Hallen, R. Yakimova, D. Panknin and W. Skorupa., Journal of Applied Physics, V. 92, #5, (2002) 2501

[10] J. F. Ziegler, J. P. Biersack and U. Littmark, TRIM97 program, IBM Corp., Yorktown, New York, 1997

[11] W. Lengauer, S. Binder, K. Aigner, P. Ettmayer, A. Guillou, J. Debuigne & G. Groboth, J. Alloys Compds., 217 (1995) 137-1

[12] K. Aigner , W. Lengauer, D. Rafaja &, P. Ettmayer, J. Alloys Compds., 215 (1994) 121-1

[13] Binary Alloy Phase Diagrams, 2nd Ed., Editor: T. B. Massalaski, H. Okamoto, P. R. Subramanian and L. Kacprzak, ASM International

[14] J. Li, J. Appl. Phys., Vol. 93, No. 11 (2003) 9072

[15] A. Chakrabarti and A. Mookerjee, J. Phys: Condensed matter, 13 (2001) 10149